POLITECNICO DI TORINO
Repository ISTITUZIONALE

Elucidating polymer interactions in the chemical recycling of mixed PET/PA6 via hydrothermal liquefaction

Original
Elucidating polymer interactions in the chemical recycling of mixed PET/PA6 via hydrothermal liquefaction / Ceragioli, G., Spezzano, E., Tito, E., Pipitone, G., Bensaid, S., Pirone, R.. - In: WASTE MANAGEMENT. - ISSN 0956-053X. - ELETTRONICO. - 227:(2027), pp. 1-14. [10.1016/j.wasman.2026.115890]

Availability:
This version is available at: 11583/3015910 since: 2026-09-25T10:03:40Z

Publisher:
Elsevier

Published
DOI:10.1016/j.wasman.2026.115890

Terms of use:

This article is made available under terms and conditions as specified in the corresponding bibliographic description in the repository

Publisher copyright

(Article begins on next page)

27 November 2026

Waste Management 227 (2027) 115890

Contents lists available at ScienceDirect

Waste Management

journal homepage: www.elsevier.com/locate/wasman

Research Paper

Elucidating polymer interactions in the chemical recycling of mixed PET/PA6 via hydrothermal liquefaction

Guido Ceragioli, Eleonora Spezzano, Edoardo Tito *, Giuseppe Pipitone, Samir Bensaid, Raffaele Pirone

Department of Applied Science and Technology, Politecnico di Torino, Corso Duca degli Abruzzi 24, 10129 Turin, Italy

ARTICLE INFO

Keywords:
Chemical recycling
HTL
Textile waste
Multi-materials
Polyester
Nylon

ABSTRACT

Hydrothermal liquefaction (HTL) in subcritical water is an emerging approach for the chemical recycling of plastics. In this work, the effects of polymer co-processing were investigated by focusing on polyethylene terephthalate (PET) and polyamide 6 (PA6), two major constituents of synthetic textile waste. A design of experiments approach was employed to quantify the influence of temperature (300–340 °C), reaction time (10–30 min), dry matter content (10–20 wt%), and blend composition (25–75% PET) on product yields. Co-processing revealed mutually influencing effects on PET and PA6 depolymerization, highlighting the critical role of polymer interactions. Terephthalic acid (TPA) derived from PET acidified the reaction medium and promoted the depolymerization of PA6; conversely, increasing PA6 content reduced TPA yields, attributed to incomplete PET hydrolysis and interactions between PET-derived species and nitrogen-containing reaction products. Monomer yields were strongly governed by operating conditions, with low dry matter content favoring water-soluble monomers, namely ethylene glycol (EG) and caprolactam (CL), and higher PET contents enhancing both the yield and purity of TPA. Within the modelled design space, optimal conditions allowed an overall monomer yield of 0.71 kg_{mon}/kg_{feed}, while tuned conditions produced maximum experimental individual yields of 79% for TPA, 57% for EG, and 62% for CL. Finally, selected operating conditions were validated using commercial PET and PA6 textile materials, showing good agreement with results obtained from model polymers. Overall, this study provides quantitative insight into PET–PA6 interactions under HTL conditions and supports the identification of operating windows for mixed textile waste valorization toward monomer recovery.

1. Introduction

Global sustainability challenges are intensified by the rising production of plastics, which currently exceeds 430 million metric tons annually and continues to grow by 2.5% per year; most of this production still derives from fossil feedstocks and is only marginally recycled (Geyer et al., 2017; Iroegbu et al., 2021; PLASTIC EUROPE, 2025). Among the available mitigation strategies, recycling represents the most immediate and practical route to reduce plastic waste accumulation. The currently dominant mechanical recycling, although relatively energy and cost effective, suffers from critical limitations. It requires clean and homogeneous waste streams, which are challenging in the case of post-consumer wastes, and suffers from downcycling phenomena (Schirmeister and Mülhaupt, 2022). In this context, chemical recycling is gaining increasing attention and Europe plans to allocate about 8 billion euros to this sector by 2030 (PLASTIC EUROPE, 2022; Van Geem, 2023).

Chemical recycling of plastics comprehends a range of approaches that differ primarily in how polymer structure is transformed and the extent of depolymerization. Some processes, such as pyrolysis, gasification, and supercritical hydrothermal liquefaction (HTL), promote extensive chain scission, converting polymers, especially polyolefins, into gaseous and liquid hydrocarbons that can serve as alternatives to fossil feedstocks for chemical production (Peti et al., 2025; Ragaert et al., 2017; Umdagas et al., 2026). Other approaches, such as solvolysis, enzymolysis, and subcritical HTL, break polymer chains into their original monomers or oligomeric intermediates suitable for repolymerization (Dogu et al., 2021; Harasymchuk et al., 2024; Yu et al., 2025).

In this context, HTL represents a particularly versatile platform, as its reaction environment and operating regime can be tailored to steer either extensive depolymerization or selective monomer recovery (Savage, 2024). HTL operates in aqueous environments (5–30 wt% dry matter, defined as the fraction of dry solids in the total water–solid

* Corresponding author.
E-mail address: edoardo.tito@polito.it (E. Tito).

https://doi.org/10.1016/j.wasman.2026.115890
Received 27 March 2026; Received in revised form 20 August 2026; Accepted 17 September 2026
Available online 22 September 2026
0956-053X/© 2026 The Author(s). Published by Elsevier Ltd. This is an open access article under the CC BY-NC-ND license (http://creativecommons.org/licenses/by-nc-nd/4.0/).

mixture) under sub- or supercritical conditions (250–450 °C, 150–250 bar) in a 5–120 min reaction time range (Boel et al., 2024). Depending on the feedstock and working conditions, HTL can lead up to four phases: solids, oil, aqueous phase (AP) and gases (dos Passos et al., 2020; Laredo et al., 2023; Umdagas et al., 2026). Under subcritical water conditions, HTL is able to convert condensation polymers that contain heteroatoms (oxygen, nitrogen, or chlorine), such as polyethylene terephthalate (PET), polyvinyl chloride (PVC), polyurethanes (PU), and polyamides (PA) (dos Passos et al., 2020; Tito et al., 2024). Conversely, polyolefins (e.g., polyethylene and polypropylene) require supercritical conditions to achieve high depolymerization efficiency (Seshasayee and Savage, 2020). This feedstock selectivity makes HTL particularly attractive when both subcritical and supercritical conditions are integrated, enabling the complete valorization of mixed plastic waste streams (dos Passos et al., 2025, 2024; Tito et al., 2023a).

Within the family of condensation polymers, polyester (e.g., PET) and nylon (e.g., polyamide 6, PA6) dominate the synthetic textile sector, representing more than 60% of total global fiber production. In particular, PET accounts for 85% of synthetic fiber production (Textile Exchange, 2024). Upon complete hydrolysis, PET is depolymerized into terephthalic acid (TPA) and ethylene glycol (EG), recovered from the solid and AP, respectively.

Operating parameters strongly influence PET depolymerization efficiency under HTL conditions. Temperature results as a critical factor: below 250 °C, depolymerization is slow and limited, 280–330 °C maximizes monomer yields, while higher temperatures (>350 °C) accelerate undesired secondary reactions (dos Passos et al., 2020). Increasing the reaction time promotes complete conversion of oligomers to monomers, though excessive durations favor secondary degradation reactions, leading to reduced monomer yields (Jaime-Azuara et al., 2023). The medium pH also plays a key role: acidic conditions favor hydrolysis, whereas neutral or basic environments lead to solubilization of terephthalates. PET hydrolysis itself, which leads to the production of TPA, causes a decrease in pH that may self-catalyze further hydrolysis (Darzi et al., 2022).

On the other hand, PA6, the second most common synthetic fiber, undergoes complete hydrolysis to yield ε-caprolactam (CL). The dense network of intra- and intermolecular hydrogen bonds between amide groups promotes PA6 high crystallinity and chemical stability, making its depolymerization under hydrothermal conditions more difficult than that of polyesters (Iwaya et al., 2006). Under such conditions, PA6 follows a reaction pathway involving amide bond hydrolysis to 6-aminocaproic acid, its reversible cyclization to ε-caprolactam, and secondary reactions leading to oligomers, ammonia and light amides (Iwaya et al., 2006; Yu et al., 2023). PA6 depolymerization is favored under higher temperatures (300–350 °C), longer reaction times (>30 min), and acidic conditions, which promote hydrolysis and enable caprolactam yields above 90% (Darzi et al., 2022; Iwaya et al., 2006).

Despite the extensive knowledge of the hydrolysis of pure PET and pure PA6, little is known about the behavior of their mixtures. Given the intrinsic complexity of real textiles, which comprise natural fibers and multiple synthetic polymers, chemical recycling must be assessed under representative feedstock conditions (Parnell et al., 2025). In this context, HTL of real textile waste has been explored for oil production from natural fibers, monomer recovery from synthetic polymers, and assessment of additive effects, with continuous processing enabling TPA recoveries exceeding 40% (Matayeva et al., 2025, 2023; Matayeva and Biller, 2021). However, these studies focused on overall process performance rather than on specific polymers interactions, which are essential for tuning process conditions toward optimized monomer recovery.

To date, polymer interactions under HTL conditions have been explicitly addressed only to a limited extent. Among the few studies, the work of Darzi et al. investigated the interaction between PET and PA6 under HTL conditions using a 600 mL Parr reactor loaded with a 3 wt% dry matter feed of pure PET, pure PA6, and a 50/50 blend, operated at 300 °C for 90 min. They found that, when co-processed, the TPA formation was inhibited (Darzi et al., 2022). More recently, de Tommaso et al. examined the hydrothermal treatment of mixed plastics representative of automotive waste, including a binary PET/PA6 blend (75/25 wt%) processed at 250 °C for 4 h. When co-processed with PA6, the yield of solid TPA decreased from 94% to 78%, an antagonism primarily ascribed to the enhanced solubilization of TPA in the aqueous phase promoted by the basicity of PA6-derived nitrogen specie (de Tommaso et al., 2026). These studies suggest that polymer interactions may strongly influence monomer production; however, their impact has so far been investigated only under a narrow set of reaction conditions, leaving unresolved how these interactions evolve across the broader operational space relevant to industrial HTL.

To fill this gap, the present work explores the behavior of PET and PA6 mixtures during different HTL conditions, focusing on how their interactions affect monomer production efficiency. A design of experiments (DoE) approach is employed to systematically investigate the influence and interactions of key process parameters, namely temperature, dry matter content, reaction time, and polymer blend composition through a continuous domain. With respect to previous studies, which addressed PET–PA6 co-processing at single discrete conditions, this work quantifies synergistic and antagonistic effects across a continuous four-dimensional operating domain, and elucidates their chemical origin through dedicated experiments in which the polymers were co-processed with their corresponding monomers. All three target monomers, namely TPA, EG and CL, are simultaneously assessed, allowing the identification of operating windows for overall monomer yield, and the results obtained with model polymers are finally validated on real textile materials. This study provides both qualitative and quantitative understanding of polymer interactions under hydrothermal conditions, offering valuable insight into the optimization of HTL for enhanced monomer yield and establishing the basis for future predictive modeling, techno-economic, and life-cycle assessments.

2. Materials and methods

2.1. Materials

PET granules (nominal size 3–5 mm) were supplied by Goodfellow, while PA6 flakes were obtained by grinding a PA6 bar purchased online using a cutting mill (SM 200, Retsch) equipped with a 3 mm × 3 mm sieve. Representative black polyester and blue polyamide 6 textile samples (Fig. S1) were purchased from commercial online retailers and ground with the same cutting mill and 3 mm × 3 mm sieve used for PA6. All the following reagents were bought from Sigma Aldrich and were used as received: sodium hydroxide (NaOH) (≥98%), sulfuric acid (H_2SO_4) (99%), acetonitrile (99.8%), formic acid (98%), dimethyl sulfoxide (DMSO) (≥99.7%), ethylene glycol (VWR, 98%), terephthalic acid (≥99%), ε-caprolactam (99%), bis(2-hydroxyethyl) terephthalate (BHET) (95%), diethylene glycol (DEG) (98%), triethylene glycol (TEG) (≥99%), benzoic acid (≥99.5%), caprolactone (97%).

2.2. HTL experimental procedure

Batch HTL experiments were conducted using 20 mL reactors, loaded with the weighed polymers and deionized water up to 10 g of total slurry, according to the composition defined by the DoE. The reactors were submerged in a preheated fluidized sand bath (Techne© SBL-2D, controller Techne© TC-9D) at setpoint temperature and for the desired reaction time. No internal stirring was provided, but agitation was provided only by sand fluidization. The reaction time for each test was measured from the moment the setpoint temperature was reached, as illustrated in Supplementary Fig. S2 and Table S1. The pressure corresponded to the autogenous pressure at the set-point temperatures. Afterwards the reactor was quenched to room temperature by immersion in water, reaching temperatures below 50 °C in less than 45 s. Gas mass

determination was performed by weight difference after venting, which resulted in negligible values.

The AP and the solid phase were separated by centrifugation. The AP was collected and stored at 4 °C. The recovered solid phase was treated with a 1 M NaOH solution and sonicated at 50 Hz for 5 min to selectively solubilize TPA and its oligomers (Agostini et al., 2022; Nouira et al., 2025; Tito et al., 2023b). The remaining insoluble material, hereafter referred to as residual solids (RS), was recovered by vacuum filtration. RS represents the fraction of solid material persisting after HTL and alkaline extraction and does not necessarily correspond to fully unreacted polymer. It may include partially depolymerized polymer fragments, re-condensed species, and other insoluble secondary products. Accordingly, the RS yield will be used as an operational parameter describing solid-phase persistence rather than as a direct measure of polymer conversion.

The alkaline liquid phase was acidified with concentrated H_2SO_4 to precipitate the TPA-rich fraction, which was recovered by vacuum filtration and comprised TPA, oligomers, and other species derived from depolymerization. All solid fractions were dried overnight at 105 °C prior to analysis.

2.3. Product characterization

The elemental composition (CHNS) of feedstock and products was determined by Elementar vario MACRO cube analyzer (Langenselbold, Germany) to conduct the carbon balances (equations in Paragraph S1 of supplementary material). Fourier Transformed Infrared (FTIR) with Bruker Tensor27 and thermogravimetric analysis (TGA) with Mettler Toledo SDTA851 were performed on virgin model plastics (granules and flakes) and textiles to enable a comparative assessment of their chemical and thermal characteristics.

The AP characterization was performed using HPLC (Shimadzu Prominence) equipped with a Rezex ROA-Organic acid H^+ (8%) column (300 · 7.8 mm); the flow rate of the mobile phase (5 mM H_2SO_4 aqueous solution) was fixed at 0.7 ml/min, the oven temperature was set at 50 °C and the run lasted 120 min. The AP samples were diluted 1:10 v/v in milliQ. Compounds were detected using a refractive index detector (RID) and a photodiode array detector (PDA), in the range 190–380 nm. The amount of TPA and BHET in TPA-rich samples were analyzed using a Kinetex C18 column (5 µm, 150 · 4.6 mm), the flow rate of the mobile phase was fixed at 1 mL/min (milliQ, acetonitrile, formic acid at a volumetric ratio 7:2:1 (Furukawa et al., 2018)), the oven temperature was set at 50 °C. 10 mg of the TPA-rich sample was diluted in 5 mL of DMSO and subsequently diluted 1:10 v/v in DMSO. The detection of the species was made by means of a PDA at 254 nm.

For CL determination and more detailed compositional characterization, AP was analyzed with a GC (Agilent 7890A GC) coupled with MS (Agilent 5975C). AP samples were diluted 1:10 v/v in milliQ. 1 µL of diluted sample was injected on a DB-WAX UI column (dimensions 30 m · 0.25 mm · 0.25 µm) in split mode with a split ratio of 50:1 and injection temperature of 240 °C. The helium flow in the column was kept constant at 1 mL/min while the temperature programming was 80 °C (2 min soak) // 5 °C/min // 250 °C (0 min soak). The identification of compounds was based on NIST 17 library and only compounds with a match factor greater than 70 were retained for subsequent manual verification of the corresponding mass spectra (Matayeva and Biller, 2022). External five-point calibration curves for quantification were prepared using purchased standards, and all experimental values fell within the corresponding calibration domains.

2.4. Evaluation of products yields

RS yield of HTL test was evaluated according to Eq. (1):

$$RS\ yield\ (\%) = \frac{m_{RS}\ (g)}{m_{PET}\ (g) + m_{PA6}\ (g)} \cdot 100 \quad (1)$$

The yields of TPA (Eq. (2)), TPA-rich fraction (Eq. (3)), EG (Eq. (4)), and CL (Eq. (5)) were calculated assuming complete depolymerization of the initial polymers according to the stoichiometric reactions reported in supplementary Fig. S3.

$$TPA\ yield\ (\%) = \frac{m_{TPA}\ (g)}{m_{TPA\ theoretical}\ (g)} \cdot 100 \quad (2)$$

$$TPA-rich\ yield\ (\%) = \frac{m_{TPA-rich}\ (g)}{m_{TPA\ theoretical}\ (g)} \cdot 100 \quad (3)$$

$$EG\ yield\ (\%) = \frac{m_{EG}\ (g)}{m_{EG\ theoretical}\ (g)} \cdot 100 \quad (4)$$

$$CL\ yield\ (\%) = \frac{m_{CL}\ (g)}{m_{CL\ theoretical}\ (g)} \cdot 100 \quad (5)$$

2.5. Design of experiment model

A DoE approach was employed to simultaneously investigate the main variables affecting the HTL process. The influence of four variables (or factors) was evaluated: dry matter (DM), reaction temperature (T), reaction time (t), and the PET concentration in the polymer blend (% PET). The selected experimental domain was intentionally designed to include both partial and near-complete depolymerization conditions, allowing the evolution of polymer interactions during HTL to be captured.

A central composite design (CCD) was adopted with three levels for each factor, resulting in 25 different experimental conditions. The central point was replicated twelve times to ensure reproducibility, while all other points were tested twice, totalizing 60 individual experiments. The levels for each factor are and the complete list of experimental conditions is reported in Supplementary Tables S2 and S3.

Multiple linear regression analysis was used to determine the coefficients (β_i) of the general quadratic equation (Eq. (6)) for each variable, thereby describing the experimental response as a function of the investigated variables. The model is reported in terms of the original (uncoded) experimental units (°C, min, wt%, %PET). Based on these equations, contour plots were generated to visualize system behavior across the continuous domain corresponding to coded levels from − 1 to 1 in Table S2. Analysis of variance (ANOVA) was also applied to evaluate the goodness of fit of the regression model.

$$\begin{aligned} Variable = {} & \beta_0 + \beta_T \cdot T + \beta_{DM} \cdot DM + \beta_{PET} \cdot \%PET + \beta_t \cdot t + \beta_{T \cdot DM} \cdot (T \cdot DM) \\ & + \beta_{T \cdot PET} \cdot (T \cdot \%PET) + \beta_{T \cdot t} \cdot (T \cdot t) + \beta_{DM \cdot PET} \cdot (DM \cdot \%PET) \\ & + \beta_{DM \cdot t} \cdot (DM \cdot t) + \beta_{PET \cdot t} \cdot (\%PET \cdot t) + \beta_{T^2} \cdot T^2 + \beta_{DM^2} \cdot DM^2 \\ & + \beta_{PET^2} \cdot \%PET^2 + \beta_{t^2} \cdot t^2 \end{aligned} \quad (6)$$

To gain deeper insights into the interaction mechanisms governing depolymerization, additional experimental points outside the original DoE design were investigated in duplicate, either as polymer blends or by replacing one or both polymers with their corresponding monomers. When these points fell within the domain defined by the DoE, they were subsequently compared with the model predictions and used as validation points.

Finally, real textile samples were analyzed in triplicate both as individual materials and blend conditions, to assess the transferability of the results obtained with model polymers. Unless otherwise stated, error bars in all figures represent ± one standard deviation of replicate experiments.

3. Results and discussion

3.1. Residual solid

The RS yield ranged from 0 to 43% (Table S4), indicating a strong

dependence on operating conditions. As shown by the contour plots reported in Fig. 1 (equation coefficients in Table S5) and ANOVA (Table S6), reaction time emerged as the most influential parameter. Increasing the reaction time consistently reduced the RS yield, indicating that, within the investigated window, conversion was predominantly governed by reaction kinetics. Under almost all conditions, the longest reaction times led to nearly complete disappearance of RS. The only exception was observed at the lowest PET content (25%) combined with the lowest temperature (300 °C), where RS were still detected after 30 min, although in reduced amounts. The influence of PET content, which followed as the second most affecting parameter, will be deeply discussed below. In agreement with previous literature reports (Jaime-Azuara et al., 2023; Yu et al., 2023), higher temperatures reduced the RS yield. This can be ascribed to the increase in hydrolysis kinetics consequent to temperature increase. The DM content showed a comparatively minor influence on RS yield. Its decrease slightly reduced the amount of RS, likely by enhancing hydrolytic depolymerization and limiting secondary condensation reaction (Boel et al., 2024).

Focusing on the effect of PET content, the contour plots show that the RS yield decreased with increasing PET content, reaching negligible residual solid at the highest %PET. This behavior can be attributed to two main factors. First, PA6 is known to exhibit higher hydrolytic resistance than PET, which stems from the different nature of their backbone linkages, namely amide bonds in PA6 versus ester bonds in PET (Baumert et al., 2024). PET hydrolysis under hydrothermal conditions has been reported to occur in less than 10 min at approximately 300 °C (Sato et al., 2006), whereas more than 30 min are required for PA6 at the same temperature (Iwaya et al., 2006). Accordingly, samples with higher PA6 fractions exhibited larger amounts of RS, whose FTIR spectra (see Fig. S4 and Table S7) resembled the characteristic signals of the polyamide, supporting that the RS arose from its incomplete hydrolysis. Nevertheless, hydrolytic resistance alone does not fully account for the observed behavior; therefore, additional experiments were performed to further elucidate PET–PA6 interactions. These tests were carried out at fixed DM content (15 wt%) and reaction time (20 min), while varying the blend composition from 0 to 100 wt% PET at 300, 320,

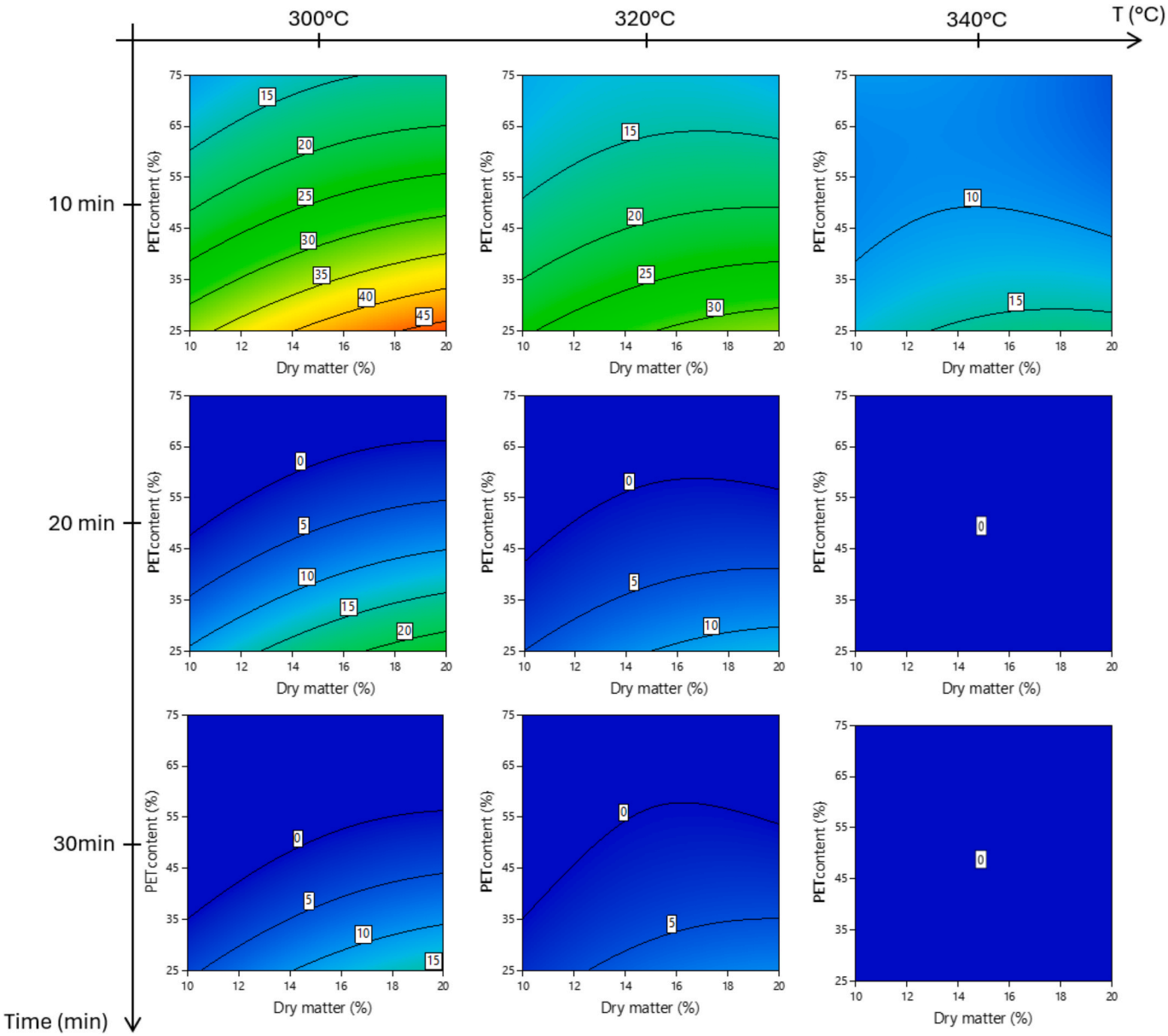

Fig. 1. Contour plot of RS yield.

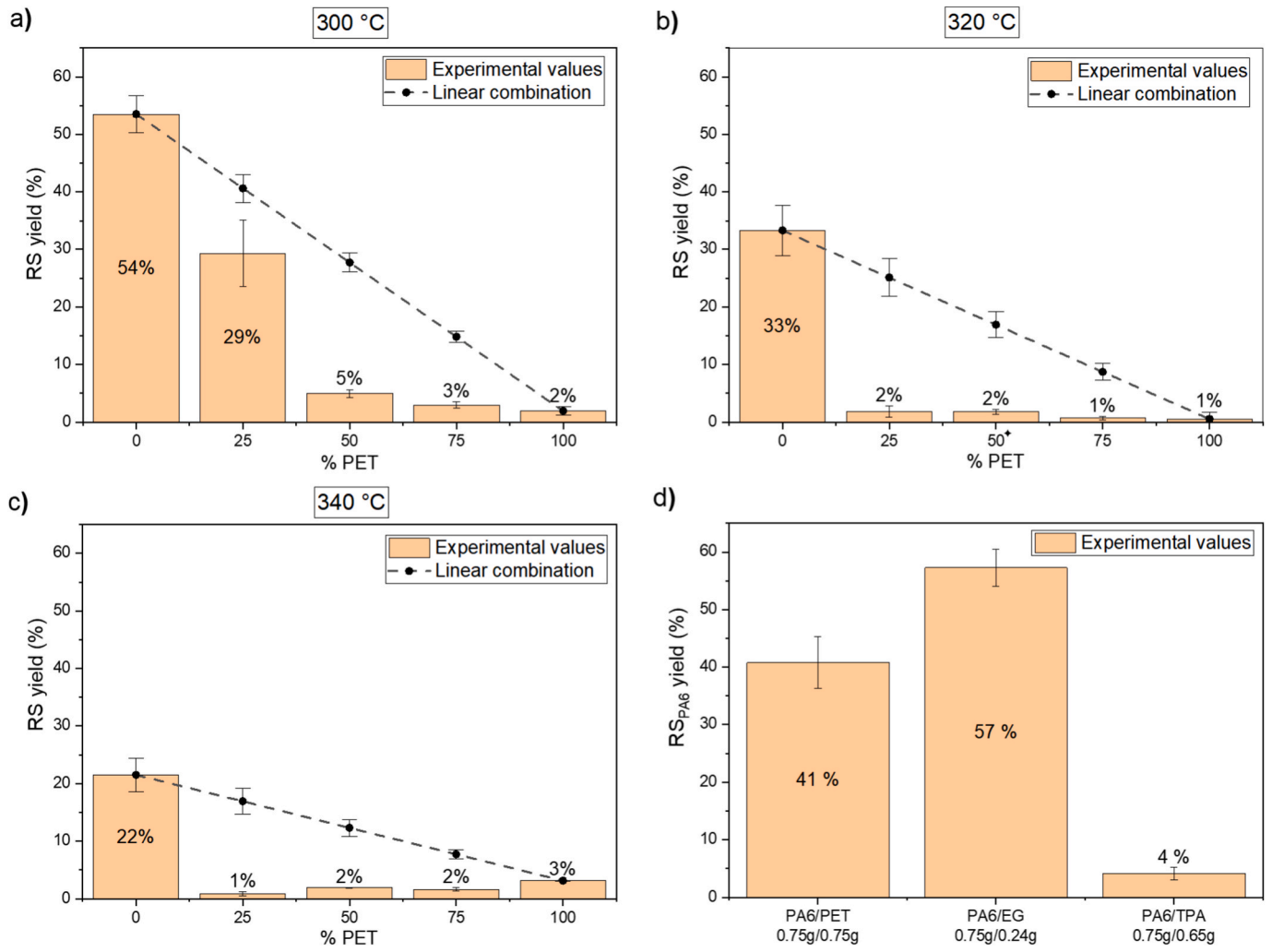

Fig. 2. Influence of PET content on RS yield at different temperatures: (a) 300 °C, (b) 320 °C (✦ has been replicated 12 times instead of 2), and (c) 340 °C. Operating conditions: reaction time 20 min, DM 15%. (d) Influence of the PA6 co-feed component (PET, EG or TPA) on RS_{PA6} yield. Operating conditions: reaction temperature 300 °C, DM 15%, reaction time 10 min.

and 340 °C (Fig. 2a–c). For each temperature, the experimental RS yields were compared to a reference behavior obtained as the linear combination of the RS yields of the pure polymers (dotted lines), which represents the expected blend response in the absence of PET-PA6 interactions. In all cases, the experimental RS yields for the blends fell systematically below this reference, evidencing a synergistic interaction between PET and PA6 that enhanced overall depolymerization relative to that expected from independent reactions. Since the experiments in Fig. 2a–c were carried out at constant overall DM content, changing the PET content also changed the absolute concentration of each polymer in the feed. Therefore, a potential alternative explanation was that the deviation from linear combination could arise from non-linear effects of polymer concentration on depolymerization. To prove this point, HTL of pure PA6 at halved DM was performed at 300 °C. The RS yield decreased compared to the 15 wt% case (Fig. 2a, equal to 54%), being equal to 36%. However, this concentration effect alone cannot explain the much larger RS yield decrease observed in the blends. Although absolute polymer concentration does play a role, the pronounced reduction in RS yield was primarily attributed to interactions between PET and PA6 during depolymerization.

To elucidate the origin of the synergistic depolymerization, additional experiments were conducted in which PA6 reacted with PET monomers added in stoichiometric amounts corresponding to PET depolymerization (Fig. S3). The results are reported in Fig. 2d as RS_{PA6} yields, defined as the mass of residual solid relative to the mass of PA6 in the feed (Eq. S10). The results clearly show that the residual solid decreased by almost ten times when PA6 was directly put in contact with TPA, rather than with PET. In contrast, when EG was used as the sole co-reactant, the RS yield increased significantly. These monomer addition experiments provide direct experimental evidence that the PET–PA6 synergy is primarily driven by TPA formation, which contributed to the acidification of the AP and consequently promoted PA6 depolymerization by accelerating amide bond cleavage, in line with the well-documented promoting effect of both mineral and organic acids on polyamide hydrolysis (Chen et al., 2010; Hocker et al., 2014; Stiegelmaier et al., 2024). Consistently, post-reaction pH measurements showed a progressive decrease in pH with increasing PET content (see Table S4).

3.2. *Terephthalic acid*

Within the investigated domain, TPA yields ranged from 18 to 79% (Table S4), and the corresponding contour plots are depicted in Fig. 3. The additional experimental points falling within the DoE domain, collected to further elucidate the effect of PET–PA6 interactions on RS yield, were also used to validate the TPA yield prediction model. The resulting parity plot (Fig. S5) shows that most validation points are closely aligned with the bisector, confirming the good predictive performance of the model.

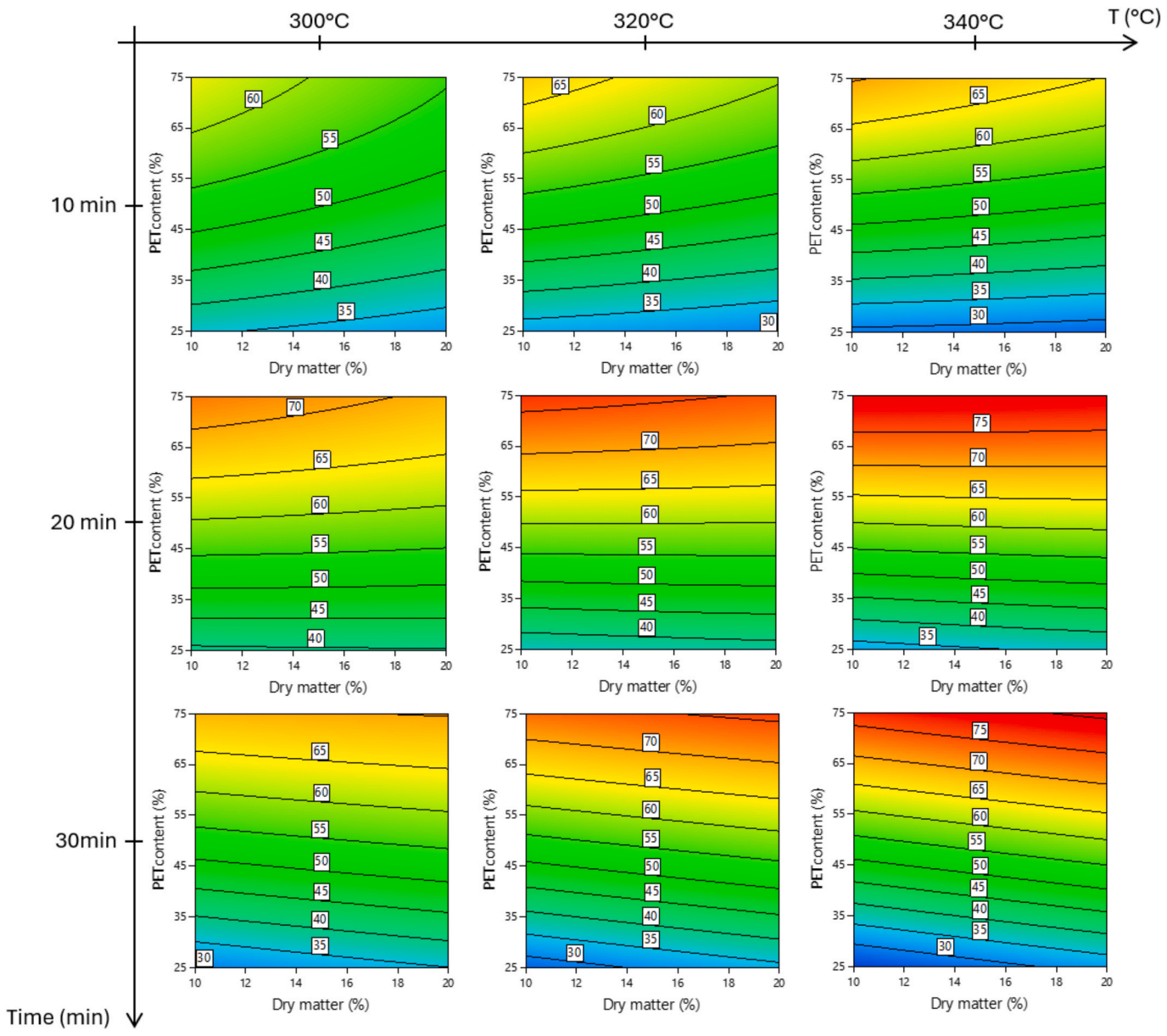

Fig. 3. Contour plot of TPA yield.

The model revealed that the PET content largely outweighed the other parameters as the most impactful on TPA yield. Across the entire domain, TPA yield increased consistently with increasing PET. This behavior was hypothesized to arise from the combination of two main effects through which PA6 influenced PET depolymerization.

First, the analysis of the TPA-rich fraction composition suggested that the presence of PA6 interfered with the complete depolymerization of PET. Indeed, while bis(2-hydroxyethyl) terephthalate (BHET), an intermediate compound formed during incomplete PET hydrolysis (Jaime-Azuara et al., 2023), was not detected in the 100% PET experiment, it was quantified in all PET/PA6 blends (see a representative HPLC chromatogram in Fig. S6). Specifically, the amount of BHET expressed as equivalent TPA (Equation S11) varied between 3 and 17% inside the DoE boundaries (Fig. S7). This effect is evidenced by the first and second columns of Fig. 4: compared to PET only, the TPA yield decreased in favor of BHET in the case of a 50%-50% PET/PA6 feed, corroborating the strong influence of PA6 in slowing PET hydrolysis. Furthermore, the TPA/BHET molar ratio showed an important increase with increasing PET content in the whole DoE domain, moving from 2 to 4 up to 14–16 (Fig. S8). This behavior may be rationalized considering the different melting points of the two polymers. Although PA6 is more recalcitrant to hydrolysis, it melts at a lower temperature than PET (160 vs 210 °C (de Tommaso et al., 2026; Jaime-Azuara et al., 2024)). It can therefore be hypothesized that molten PA6 may partially coat the PET surface within the reactor, limiting the accessibility of water to PET, thus slowing its hydrolysis. Nevertheless, this interpretation should be regarded as a hypothesis, since no direct experimental evidence of this phenomenon was obtained in the present study.

The second effect of PET content on TPA yield could be attributed to the presence of nitrogen-containing molecules, such as amides like 4-carbamoylbenzoic acid (TPAm-N1) and terephthalamide (TPAm-N2), or similar species. Elemental analysis (Table S8) revealed the presence of nitrogen in the TPA-rich fraction, which increased with decreasing PET contents (Fig. S9). Nitrogen incorporation is likely linked with intermediates formed during PA6 hydrolysis that could have reacted with TPA through amidation reactions, ultimately leading to reduced TPA yield (Darzi et al., 2022; Matayeva et al., 2025). A combined analysis of TPA yield (Fig. 3) and nitrogen content in the TPA-rich fraction (Fig. S9)

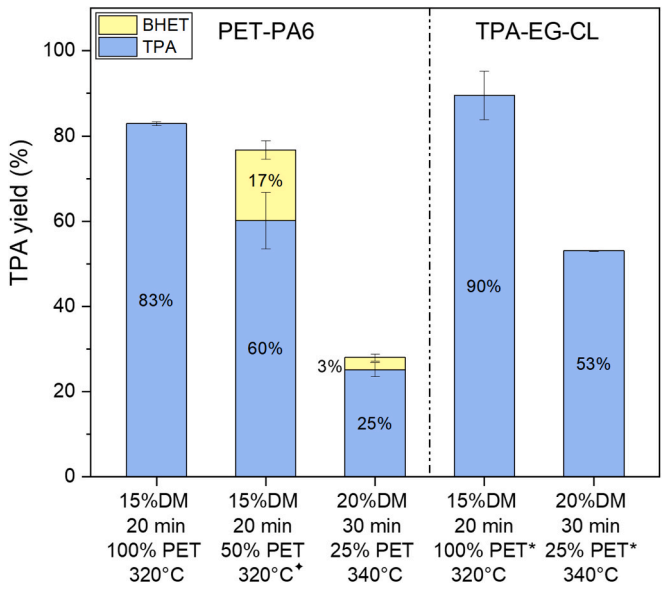

Fig. 4. Influence of specific reaction conditions on TPA and BHET yield (✦ has been replicated 12 times instead of 2). Asterisks (*) indicate values expressed as monomer equivalents relative to the initial polymer mass.

highlights a complementary behavior that depends on reaction temperature and residence time. At moderate temperatures (≈300–320 °C), decreasing PET content was associated with both a reduction in TPA yield and an increase in nitrogen incorporation in the TPA-rich fraction. This trend is consistent with the Van Krevelen diagrams (Fig. S10), where increasing PA6 content shifted the elemental composition of the TPA-rich fraction toward that of the proposed amides (TPAm-N1/TPAm-N2), whose identification would however require dedicated LC-MS/MS or NMR analyses. At higher temperatures and longer residence times, TPA yield still decreased while the nitrogen content in the TPA-rich fraction was reduced, suggesting a different partitioning behavior of nitrogen-containing species. Under these conditions, nitrogenated compounds were likely increasingly solubilized in the AP rather than retained in the TPA-rich solid phase. The PA6 inhibition effect on TPA is illustrated by comparing the second and third columns of Fig. 4: an increase in PA6 content, reaction time and temperature resulted in a marked decrease in TPA yield from 60% to 25%.

The PET-PA6 interaction mechanism was further confirmed by additional experiments performed with an equivalent amount of PET monomers and PA6. The last two columns of Fig. 4 show a decrease in TPA yield that follows the same trend observed in the polymer–polymer system, although to a slightly lower extent. These results confirm that the decrease in TPA yield is not solely related to slower PET depolymerization but is consistent with a degradation mechanism induced by CL-derived nitrogen compounds affecting TPA yield.

An additional contribution may arise from the enhanced solubility of TPA itself: as proposed by de Tommaso et al., basic nitrogen species released during PA6 hydrolysis can raise the medium pH, shifting TPA toward its soluble deprotonated forms and reducing its recovery as a solid (de Tommaso et al., 2026). This is consistent with the higher post-reaction pH measured at the lowest PET contents (Table S4).

The TPA-rich yield (contour plots in Fig. S11) exhibited trends analogous to those of the TPA yield, though with reduced magnitude. TPA-rich yields exceeding 100% can be attributed to the presence of non-TPA components within the TPA-rich fraction. While TPA yield decreases across the investigated conditions, the TPA-rich yield shows a more marked reduction at longer reaction times and higher temperatures. This behavior is consistent with the hypothesis of progressive solubilization of TPA-derived, nitrogen-containing species, in line with the complementary trends previously discussed between TPA yield and nitrogen content in the TPA-rich fraction.

3.3. Ethylene glycol

The EG yield contour plots are shown in Fig. 5 (model equation in Table S5, ANOVA in Table S6), while the corresponding experimental values are reported in Table S4 and ranged within the domain from 18 to 57%. The parity plot in Fig. S12 with the additional experiments used as validation points confirmed that the model captures the overall trends, though with lower accuracy with respect to TPA.

Among the operating variables, DM was the most influential factor, as its increase systematically reduced EG yield. Interestingly, this behavior differed from TPA, whose yield did not show the same dependence on DM, even though EG and TPA are co-products of PET hydrolysis. Therefore, the decoupling suggests that, while hydrolysis may proceed, secondary conversion pathways involving EG may occur under these conditions (Boel et al., 2024; Čolnik et al., 2022).

A first hypothesis is EG condensation to diethylene glycol (DEG). However, although DEG was the third most abundant compound identified in the AP after CL and EG, its yield also decreased with increasing DM (see Fig. S13, where DEG was expressed as equivalent EG yield, according to Eq. S12). Consistently, the EG/DEG molar ratio was essentially insensitive to DM (Fig. S14), except under very mild conditions (10 min, 300 °C), where an increase in the EG/DEG ratio suggested a kinetic limitation in the formation of DEG. Outside of this operating range, EG/DEG consistently remained around 13–16 mol/mol. DEG formation is therefore more likely attributable to its incorporation within the PET polymeric structure, whose content typically ranges from ~15 to 40 mol/mol EG/DEG, since DEG contributes to modifying the polymer glass transition (Di Lorenzo, 2024; Patkar and Jabarin, 1993).

A possible hypothesis is that part EG conversion could be ascribed to secondary pathways reported in the literature, such as oxidative degradation of EG to low-molecular-weight acids and aldehydes, or cyclic condensation under harsh conditions (Čolnik et al., 2021; Jaime-Azuara et al., 2023). This hypothesis is corroborated by the numerous compounds identified in the AP, as later discussed in Paragraph 3.5.

The EG behavior as a function of DM may also be explained by its retention in oligomeric structures as BHET detected in the TPA-rich fraction, which accounted between 6 and 33% as EG yield equivalents (Eq. S14, contour plot in Fig. S15). This interpretation is supported by the decreasing trend of the EG/BHET mol/mol ratio showed in Fig. S16. This effect was particularly evident around 10% DM, where the EG/BHET was maximized. Hence, it is possible that a higher DM led to a higher interaction between PET and PA6, with the latter slowing the complete hydrolysis of the former. However, this mechanism alone cannot fully account for the overall DM effect, which may additionally stem from interactions with CL at high concentrations, as will be discussed in Paragraph 3.4.

PET content also played a significant role in EG yield, as its increment improved EG yields especially at low reaction time. Further analysis investigated such behavior under the lowest EG yield conditions inside the domain. In those experiments, it has been systematically compared polymer–polymer, polymer–monomer, and monomer–monomer mixtures (Fig. S17) to determine whether the EG yield drop was driven by (i) secondary reactions involving released monomers/products or (ii) polymer–polymer interactions during depolymerization. PET–PA6 system resulted in low EG yield (21%); in contrast, when PET was processed alone under equivalent conditions (1 g PET in 9 g water, explanation in Paragraph S2 of supplementary material), the EG yield increased to 66%, with 6% more retained in the form of DEG (expressed according to Eq. S12). A similar EG yield (62%) was obtained with a PET-CL mixture, suggesting that a direct interaction with caprolactam could not be the cause for EG yield decrease. Interestingly, when equimolar amounts of PET monomers (TPA and EG) reacted either alone or

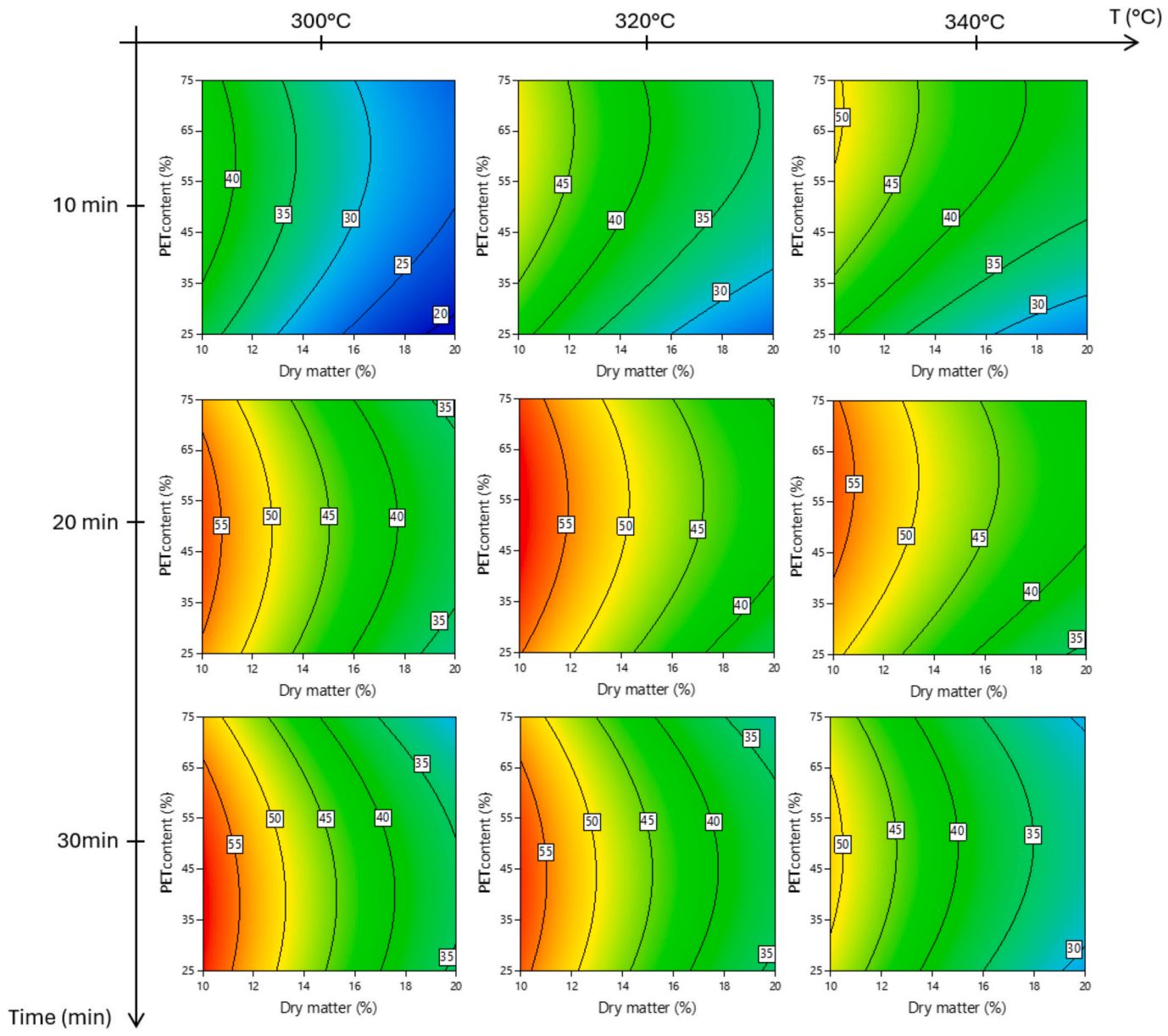

Fig. 5. Contour plot of EG yield DoE.

with CL or PA6, EG yielded 89–94%, indicating nearly complete monomer yield and the absence of secondary reactions. Comparison of these EG yields with the corresponding TPA yields (Fig. S17) reveals similar trends for both monomers, further corroborating that the yield decrease originates from impaired depolymerization. These results suggest that in mild conditions, where EG yield is minimum, it was not affected by its direct interaction with PA6 or its CL monomer, but rather by interaction between PET and PA6 during their depolymerization. In this scenario, PET depolymerization initiates while PA6 remains more recalcitrant, likely slowing PET conversion and promoting partial retention of EG in oligomeric TPA-derived species. This behavior is consistent with the previously discussed hypothesis that molten PA6, due to its lower melting point, may partially coat the PET surface, reducing its accessibility to water and thus hindering its hydrolysis.

Overall, the explained EG in this study (description in Eq. S14 and contours plot in Fig. S18) varied between 29 and 89%.

The EG general behavior could be interpreted as the complex result of a coupled effect of soluble compound concentration into the AP, kinetics and polymer–polymer interactions. Under mild conditions, EG would tend to remain partially retained within oligomeric PET structures, whose depolymerization could be slowed by the presence of PA6, particularly at high DM contents where overall conversion is less favored (Section 3.1.1). Conversely, at long time and temperature, EG and its intermediates might be increasingly involved in secondary reactions with compounds originating from PA6 depolymerization, with these pathways potentially enhanced at higher DM contents due to increased reactant concentrations.

3.4. Caprolactam

Contour plots related to CL yields are shown in Fig. 6 (relative equation in Table S5 and ANOVA in Table S6). Experimental values are reported in Table S4 and ranged from 19% to 62% within the investigated domain, while the parity plot shown in Fig. S19 demonstrates good agreement between the predicted and experimental values. Among the factors examined, DM, temperature, and reaction time were the most significant for CL yield, with similar importance (Table S6). Specifically, lower DM, higher reaction temperatures, and longer reaction times

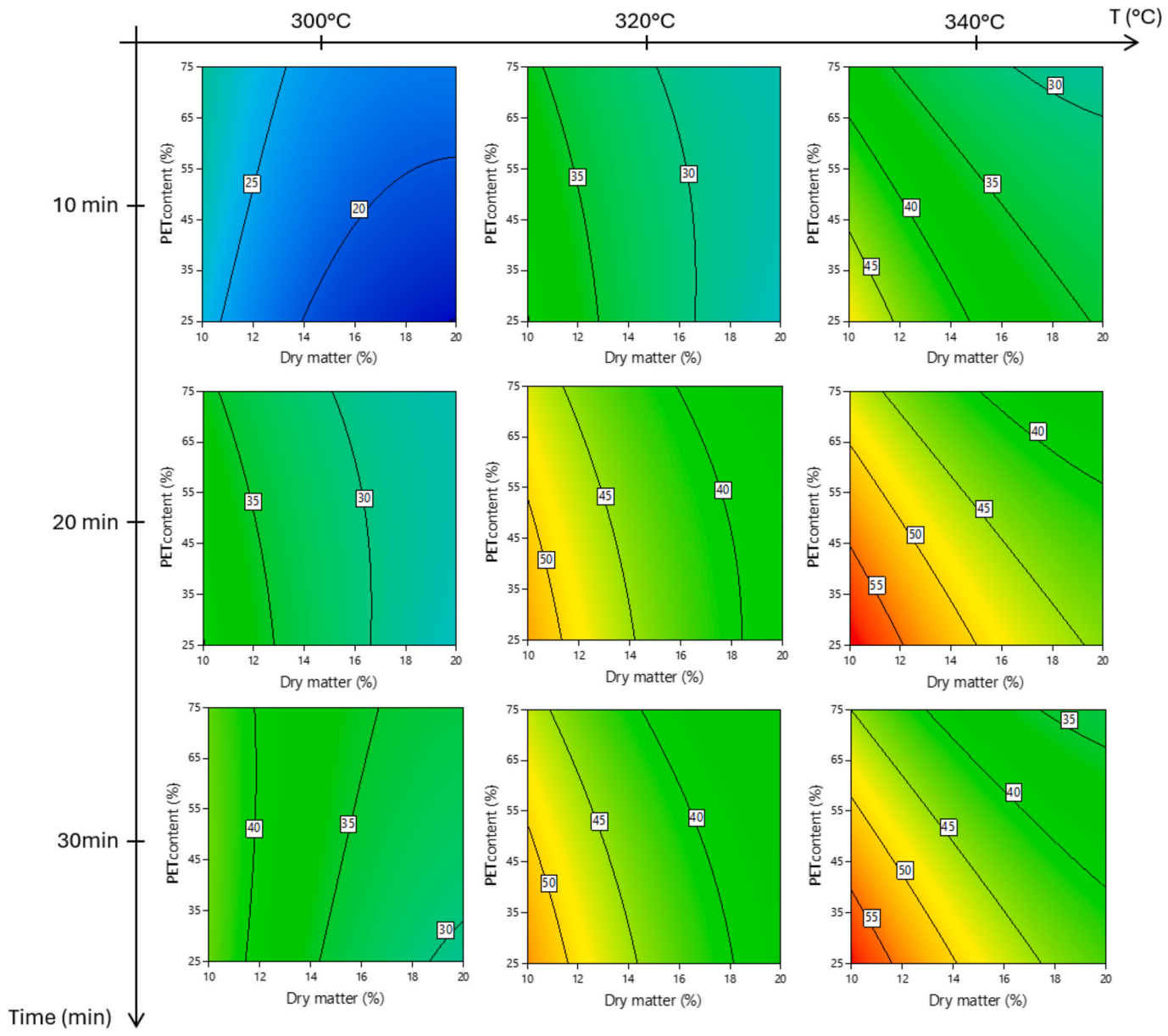

Fig. 6. Contour plot of CL yield.

enhanced CL yield, likely by promoting PA6 hydrolysis. This interpretation is supported by the opposite trends observed for RS (Paragraph 3.1), which was identified as incompletely converted PA6. Moreover, a similar decreasing trend in CL and EG yields with increasing DM was observed, suggesting that the PET–PA6 interactions proposed in Paragraph 3.3 may reduce the yield of both monomers.

PET content was the least influential variable, with its strongest effects observed at higher temperatures. Near 340 °C, where the beneficial effect of PET on PA6 depolymerization becomes negligible, increasing PET content slightly decreased CL yield. This behavior can be explained by the fact that the formed CL may undergo secondary interactions with PET-derived degradation products, similarly to the mechanism discussed for TPA yield. As the relative CL concentration decreases at higher PET contents, these interactions become proportionally more significant, resulting in a stronger decrease in CL yield.

Some compound directly derived from CL were identified in the AP through HPLC and GC–MS analyses. Among these species, caprolactone was detected at concentrations ranging from 0 to 3.91 g/L. It may originate from the cyclization of 6-hydroxyhexanoic acid, which can form under hydrothermal conditions via transformation of aminocaproic acid (ACA). In addition, 5-hexenoic acid, produced through ACA deamination was identified together with several five-membered cyclic compounds derived from carboxylic acids. The remaining unrecovered fraction of caprolactam may also be associated with formation of oligomeric species, including linear and cyclic PA6 oligomers (Yu et al., 2023), which could not be quantified with the analytical methods employed. Previous studies have reported that these species can be present in significant amounts, particularly at the short reaction times investigated in this work (Iwaya et al., 2006).

Finally, it must be highlighted that, shortly after storage, sediment formation was observed in the aqueous phase (Fig. S20-left), as also reported in the literature (dos Passos et al., 2025; Yu et al., 2023). Stability tests conducted with a specific sample showed that CL concentration slightly decreased over time (Fig. S21). Additional stability tests performed with CL alone showed no sediment formation (Fig. S20-right), indicating that the observed degradation did not involve only CL, but it necessitates also the presence of other soluble species in the post-reaction AP. Hence, these observations suggest that the model may underestimate

the actual caprolactam concentration immediately after reaction, highlighting the need for further studies on CL stability in the AP phase.

3.5. Carbon balances and optimal process operating conditions

The carbon balance and its distribution among the different phases are summarized in Fig. 7a, where the experimental conditions within the DoE are grouped according to PET content and process temperature. Overall carbon closure ranged from 68 to 96%, as commonly observed in HTL processes (Matayeva and Biller, 2022). A clear dependence of carbon fate on blend composition was observed: samples with higher PET content exhibited significantly improved carbon closure compared to PA6-rich systems. This behavior is attributed to the presence and instability of AP-soluble species, predominantly CL-derived, which during storage underwent oligomerization and repolymerization, leading to sediment formation in the AP samples, as also observed by dos Passos et al. (2025). Since residue formation occurred prior to analysis and only the soluble fraction was quantified, the carbon recovered in the AP could be underestimated (Matayeva and Biller, 2022). The hatched segments in the bars of Fig. 7a highlight the significant contribution of

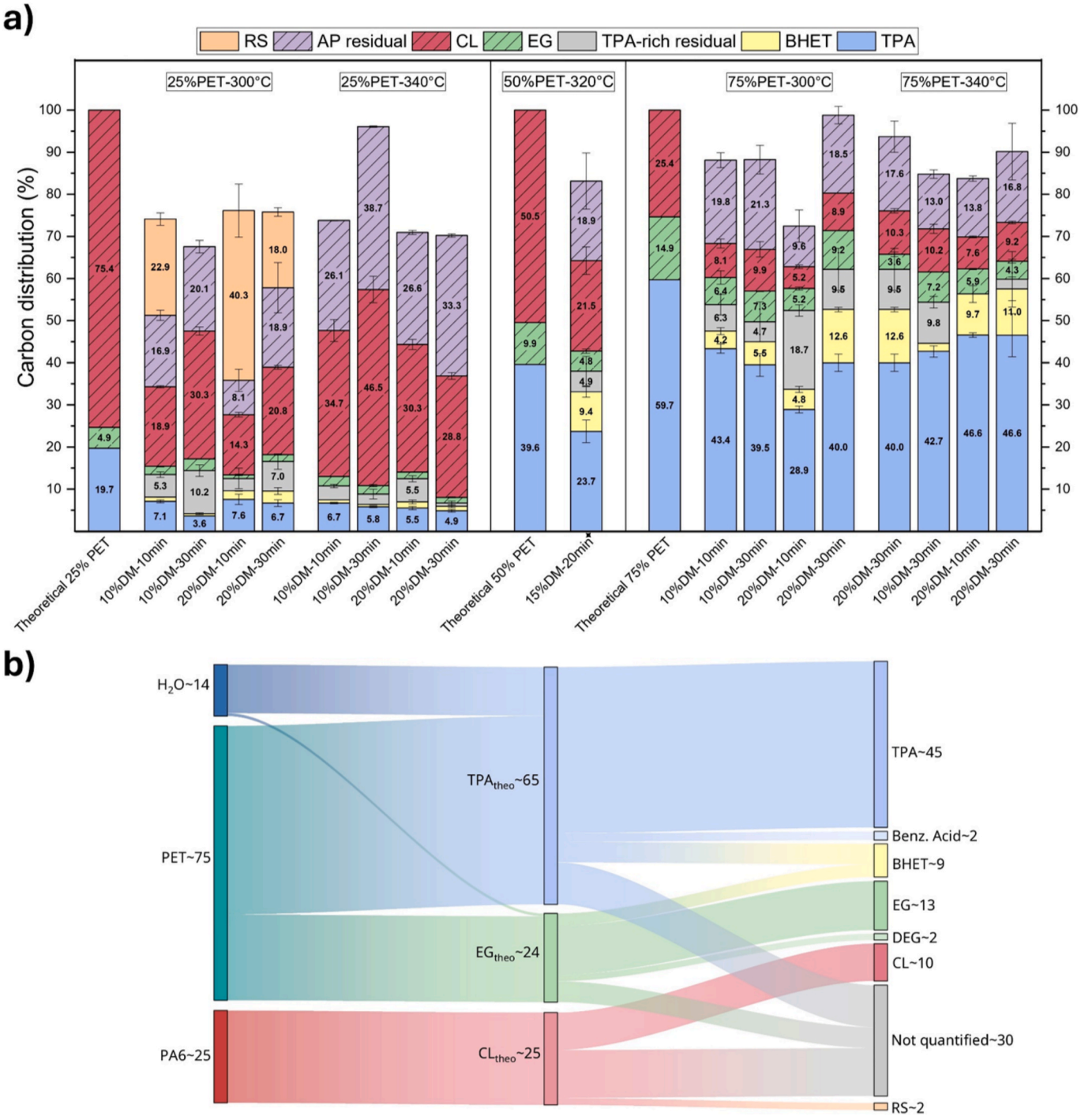

Fig. 7. (a) Carbon balances of doe condition inside the model domain (✦ has been replicated 12 times instead of 2). Internal diagonal line pattern refers to carbon inside AP. Theoretical conditions refer to the carbon distribution among TPA, EG, and CL assuming complete hydrolysis. (b) Sankey diagram of mass distribution of a representative experimentally tested condition at 10% DM/10 min/75% PET/340 °C.

AP carbon across all conditions, and substantial fraction of unassigned carbon in the AP (purple bars). Indeed, the sum of carbon as CL and EG ranged between 34 and 71% of the total carbon experimentally quantified in the AP, indicating the significant presence of numerous additional AP-soluble compounds, likely generated through secondary reactions. Among these, benzoic acid, produced by decarboxylation of TPA, was identified (3% to 9%, expressed as TPA equivalent (eq. S15)). Other water-soluble species may originate from interactions between TPA and PA6-derived nitrogen species, as reported in Paragraph 3.2, while others may derive from the degradation of EG and, in particular, from CL-derived molecules as discussed in paragraphs 3.3 and 3.4 (Darzi et al., 2022; Matayeva et al., 2025; Yu et al., 2023). To improve the identification of additional light compounds in the AP, GC–MS equipped with a headspace sampler was performed (Fig. S22). This analysis confirmed the presence of highly volatile compounds such as acetaldehyde, acetone, ethanol, and 1,4-dioxane, which are EG dehydration and condensation products.

Within the investigated design space, the DoE-based response-surface analysis further enabled the identification of operating conditions that maximize the overall recoverable monomer mass from the mixed PET/PA6 feedstock (see Eq S16). Conditions of 340 °C, 10 wt% DM, 75% PET in the blend, and a reaction time of 20 min were identified as optimal, predicting an overall monomer yield of 0.77 kg_{mon}/kg_{feed} (80% TPA yield, 56% EG yield, 47% CL yield). Experimental validation under these conditions resulted in similar TPA yields but slightly lower EG and CL yields (79% TPA, 47% EG, and 35% CL), corresponding to an overall monomer yield of 0.71 kg_{mon}/kg_{feed}. These discrepancies can be considered reasonable given the substantial model deviations shown in Fig. S23. Furthermore, examination of the experimental conditions closest to the predicted optimum revealed a significant overlap of the associated error bars (Fig. S23), despite yielding a lower overall monomer production (0.69 kg_{mon}/kg_{feed}).

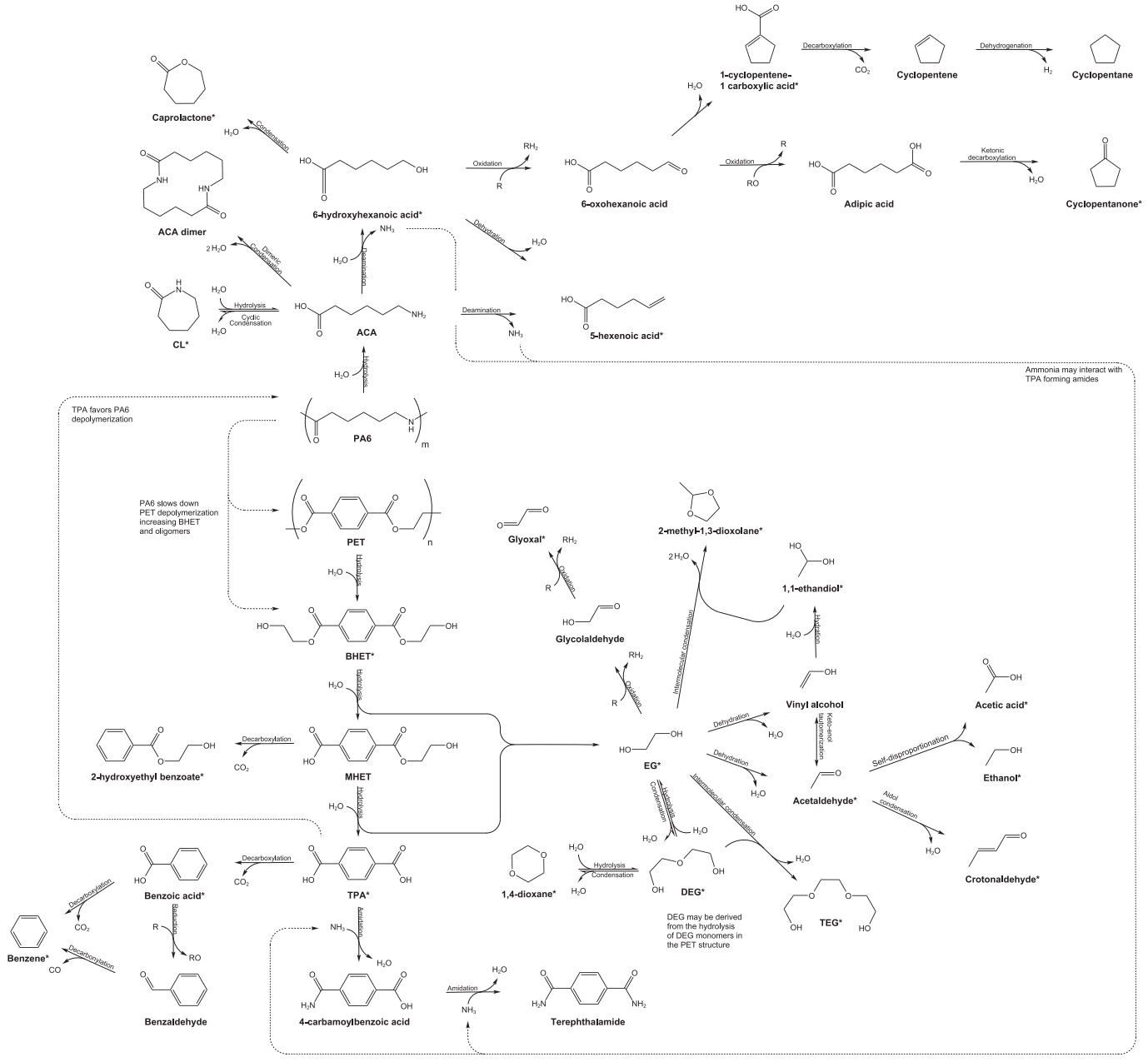

Fig. 8. Proposed reaction mechanisms and interactions during the HTL of a mixture of PET and PA6. Molecules experimentally observed in this work are labelled with an asterisk (*).

It should be highlighted that these optimal conditions should be interpreted within a laboratory-scale optimization context and may present limitations when scaled up to industrial operation. In particular, dry matter content strongly influences HTL economics, as higher solids loadings improve thermal efficiency (Snowden-Swan et al., 2016). However, increasing the dry matter also reduces slurry pumpability (Edifor et al., 2020), representing a key constraint for continuous operation. Similarly, operating at the upper temperature range and longer residence times, while favorable for monomer yields, may increase energy demand and capital costs at larger scale (Ceragioli et al., 2025). Furthermore, downstream processing represents a bottleneck. Both CL and EG are obtained at relatively low concentrations in the aqueous phase (up to ~8 wt% and ~2.5 wt%, respectively), necessitating efficient separation and concentration strategies (Dhale et al., 2004; Minor et al., 2023). Additionally, TPA must meet commercial-grade specifications for PET repolymerization (Lee et al., 2021). Therefore, it should be emphasized that the optimum identified in this study may shift under industrial-scale conditions, where processability, separation requirements, and operational considerations become critical factors.

A Sankey diagram in Fig. 7b was employed to visualize product distribution at an experimentally tested operating point close to the region of maximum monomer yield predicted by the DoE model. According to GC–MS and literature reports, the non-quantified components mainly comprise mono(2-hydroxyethyl) terephthalate (Jaime-Azuara et al., 2023), triethylene glycol (GC–MS), acetaldehyde (GC–MS headspace), 1,4-dioxane (GC–MS headspace), and ethanol (GC–MS headspace) from PET, and cyclic caprolactam dimer (Yu et al., 2023), ε-aminocaproic acid (GC–MS), ε-caprolactone (GC–MS) and cyclopentane/ene from PA6 (Darzi et al., 2022). A proposed reaction network, based on the molecules experimentally observed in this work and those reported in the literature, is presented in Fig. 8, highlighting the interaction mechanisms between PET and PA6.

3.6. Analysis on real textiles

As a preliminary step prior to the co-liquefaction experiments, the selected commercial textiles were compared with their corresponding model polymers (PET and PA6). As shown in Supplementary, TGA (Fig. S24), CHNS (Fig. S25), and FTIR analyses (Fig. S26) demonstrated a near-complete overlap between the textiles and the model polymers, confirming their chemical and structural equivalence and their suitability as reference materials.

Five operating conditions derived from those previously explored with the pure polymers were selected to investigate the behavior of real textiles. Two reference cases, corresponding to 0% PET and 100% PET, were examined under intermediate operating conditions (15% DM, 20 min, 320 °C), allowing a direct comparison between each textile sample and its corresponding model polymer. Three additional representative conditions for PET/PA6 blends were selected to evaluate the yields of all target monomer (TPA, EG, and CL). These tests used the same low DM content (10%), aimed at enhancing the yield of water-soluble monomers (EG and CL), and high PET content (75% PET), chosen to mitigate undesired polymer–polymer interaction effects, while varying the temperature–time conditions. One test was performed at lower temperature and longer reaction time (300 °C, 30 min), intended to ensure sufficient depolymerization of both polymers. A second test was performed at higher temperature and shorter reaction time (340 °C, 10 min), selected to limit secondary undesired reactions. A third test was conducted under the conditions identified as optimal for monomer yield (340 °C, 20 min). Together, these conditions were chosen to cover a broad region of the model domain while maintaining satisfactory monomer recoveries.

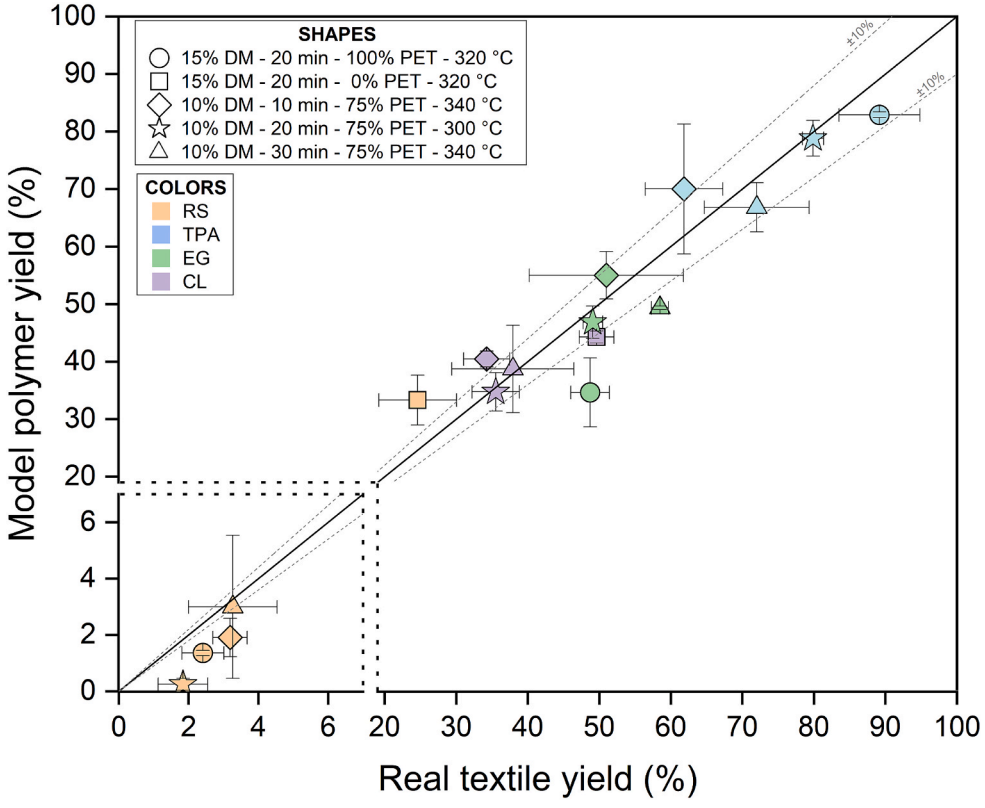

Fig. 9. Comparison of experimentally-obtained product yields from textiles and model polymers under different conditions. Dotted lines refer to ±10% deviation from bisector.

The results of HTL experiments on synthetic textiles are presented in Fig. 9 using a parity plot, where product yields obtained from textile samples are directly compared with those measured for the corresponding model polymers under identical operating conditions. In all cases the RS, TPA, EG and CL yields obtained from the real textile clustered close to the parity line, indicating a good agreement with model polymers. A slight deviation is observed at low RS yields (near the origin), where textile samples tend to produce marginally higher RS values under conditions generating only limited amounts of RS. This effect may be attributed to the higher inorganic content in the real textile feedstocks (see TGA in Fig. S24). At higher yield values, the most notable deviations are observed for RS and EG. Specifically, for the low-RS region, the RS yield for pure PA6 is lower in the real textile than in the model polymer (25% vs 33%), whereas for pure PET, the textile shows a higher EG yield (49% vs 35%). These discrepancies may arise from the presence of dyes (see Fig. S1), additives, impurities, or textile-processing effects. Nonetheless, a strong overall correlation between textile samples and model polymers is observed, particularly for mixed feedstocks, indicating that the trends identified in the DoE based on model polymers are also applicable to real textile systems.

4. Conclusions

This study demonstrates that PET–PA6 co-processing under HTL conditions is strongly governed by polymer–polymer interactions, which significantly affect depolymerization pathways and monomer yields. The DoE-based approach, combined with mechanistic experiments, enabled the identification of quantitative relationships between operating variables and monomer yields, shedding light on previously unexplored phenomena. PET promoted PA6 depolymerization through acidification of the reaction medium associated with terephthalic acid formation, whereas increasing PA6 content negatively affected TPA production, likely due to reactions with nitrogen-containing species. EG yields were mainly influenced by dry matter content. Control experiments demonstrated that EG was not directly consumed alone or in the presence of other monomers. Its incomplete production was therefore attributed to a combination of incomplete PET hydrolysis driven by polymer–polymer interactions and secondary reactions occurring during co-processing. CL yields increased with temperature and reaction time, while decreasing at higher DM, likely due to oligomer retention and secondary transformations occurring in the AP phase.

Based on the model responses, the optimal operating conditions for overall monomer mass yield were at 340 °C, 10 wt% DM, 75% PET, and 20 min, which experimentally yielded 79% TPA, 35% CL, 47% EG, and an overall monomer mass yield of 0.71 kg_{mon}/kg_{feed}. Validation experiments performed on commercial textiles also confirmed a generally good agreement with model polymer behavior, supporting the applicability of the developed approach to realistic feedstocks.

Overall, this work highlights that mixed-polymer HTL behavior cannot be extrapolated from individual plastics and demonstrates the importance of accounting for polymer interactions when designing HTL processes targeting selective monomer recovery from realistic textile waste streams. The quantitative correlations and predictive maps reported herein can support future scale-up studies which will need to additionally consider process-economic and engineering aspects.

Declaration of AI-assisted technologies in the manuscript preparation process

During the preparation of this work, the authors used ChatGPT solely to assist in revising grammar, language, and readability. The tool was not used for generating scientific content or interpretations. After its use, the authors thoroughly reviewed and edited all text, and they take full responsibility for the final content of the publication.

CRediT authorship contribution statement

Guido Ceragioli: Writing – review & editing, Writing – original draft, Visualization, Methodology, Investigation, Formal analysis, Data curation, Conceptualization. **Eleonora Spezzano:** Investigation, Formal analysis, Data curation. **Edoardo Tito:** Writing – review & editing, Visualization, Supervision, Methodology, Data curation, Conceptualization. **Giuseppe Pipitone:** Writing – review & editing, Visualization, Validation, Supervision, Methodology, Data curation, Conceptualization. **Samir Bensaid:** Writing – review & editing, Validation, Supervision, Project administration, Funding acquisition, Conceptualization. **Raffaele Pirone:** Writing – review & editing, Validation, Supervision, Project administration, Funding acquisition, Conceptualization.

Declaration of competing interest

The authors declare that they have no known competing financial interests or personal relationships that could have appeared to influence the work reported in this paper.

Appendix A. Supplementary data

Supplementary data to this article can be found online at https://doi.org/10.1016/j.wasman.2026.115890.

Data availability

The data that support the findings of this study are available from the corresponding author upon reasonable request.

References

Agostini, I., Ciuffi, B., Gallorini, R., Rizzo, A.M., Chiaramonti, D., Rosi, L., 2022. Recovery of terephthalic acid from densified post-consumer plastic mix by HTL process. Molecules 27. https://doi.org/10.3390/molecules27207112.

Baumert, B., Meinert, H., Cziegler, C., Terholsen, H., Bayer, T., Bornscheuer, U.T., 2024. Promiscuous acyltransferases for ester and amide synthesis in aqueous solution. Catal. Today. https://doi.org/10.1016/j.cattod.2024.114925.

Boel, M.J., Wang, H., AL Farra, A., Megido, L., González-LaFuente, J.M., Shiju, N.R., 2024. Hydrothermal liquefaction of plastics: a survey of the effect of reaction conditions on the reaction efficiency. React. Chem. Eng. 10.1039/d2re00510g.

Ceragioli, G., Schuck, C.E., Zoppi, G., Pipitone, G., Anastasakis, K., Bensaid, S., Pirone, R., Biller, P., 2025. Development of an integrated hydrothermal liquefaction and wet oxidation process: a pathway for an autothermal biorefinery. J. Clean. Prod. 521. https://doi.org/10.1016/j.jclepro.2025.146242.

Chen, J., Li, Z., Jin, L., Ni, P., Liu, G., He, H., Zhang, J., Dong, J., Ruan, R., 2010. Catalytic hydrothermal depolymerization of nylon 6. J. Mater. Cycles Waste Manag. 12, 321–325. https://doi.org/10.1007/s10163-010-0304-y.

Čolnik, M., Knez, Ž., Škerget, M., 2021. Sub- and supercritical water for chemical recycling of polyethylene terephthalate waste. Chem. Eng. Sci. 233. https://doi.org/10.1016/j.ces.2020.116389.

Čolnik, M., Pečar, D., Knez, Ž., Goršek, A., Škerget, M., 2022. Kinetics study of hydrothermal degradation of pet waste into useful products. Processes 10. https://doi.org/10.3390/pr10010024.

Darzi, R., Dubowski, Y., Posmanik, R., 2022. Hydrothermal processing of polyethylene-terephthalate and nylon-6 mixture as a plastic waste upcycling treatment: a comprehensive multi-phase analysis. Waste Manag. 143, 223–231. https://doi.org/10.1016/j.wasman.2022.03.002.

de Tommaso, J., Gaillard, A., Mattio, E., Ardizzone, C., Leybros, A., 2026. Hydrothermal recycling of step and chain growth mixed plastics under sub- and supercritical conditions: chemical synergies, and antagonisms. Waste Manag. 213. https://doi.org/10.1016/j.wasman.2026.115362.

Dhale, A.D., Myrant, L.K., Chopade, S.P., Jackson, J.E., Miller, D.J., 2004. Propylene glycol and ethylene glycol recovery from aqueous solution via reactive distillation. Chem. Eng. Sci. 59, 2881–2890. https://doi.org/10.1016/j.ces.2004.02.018.

Di Lorenzo, M.L., 2024. Crystallization of poly(ethylene terephthalate): a review. Polymers (Basel). https://doi.org/10.3390/polym16141975.

Dogu, O., Pelucchi, M., Van de Vijver, R., Van Steenberge, P.H.M., D'hooge, D.R., Cuoci, A., Mehl, M., Frassoldati, A., Faravelli, T., Van Geem, K.M., 2021. The chemistry of chemical recycling of solid plastic waste via pyrolysis and gasification: state-of-the-art, challenges, and future directions. Prog. Energy Combust. Sci. https://doi.org/10.1016/j.pecs.2020.100901.

dos Passos, J.S., Glasius, M., Biller, P., 2020. Screening of common synthetic polymers for depolymerization by subcritical hydrothermal liquefaction. Process Saf. Environ. Prot. 139, 371–379. https://doi.org/10.1016/j.psep.2020.04.040.

dos Passos, J.S., Lorentz, C., Laurenti, D., Royer, S.J., Chontzoglou, I., Biller, P., 2024. Hydrothermal liquefaction of plastic marine debris from the North Pacific Garbage Patch. Resour. Conserv. Recycl. 209. https://doi.org/10.1016/j.resconrec.2024.107822.

dos Passos, J.S., Skibsted, S.K.G., Biller, P., 2025. Enhancing recycling of polyamide 6 and polyethylene multilayer plastics through sequential hydrothermal liquefaction. Energy Fuels 39, 571–576. https://doi.org/10.1021/acs.energyfuels.4c04589.

Edifor, S.Y., van Eyk, P., Biller, P., Lewis, D.M., 2020. The influence of feedstock characteristics on processability of biosolid slurries for conversion to renewable crude oil via hydrothermal liquefaction. Chem. Eng. Res. Des. 162, 284–294. https://doi.org/10.1016/j.cherd.2020.08.016.

Furukawa, M., Kawakami, N., Oda, K., Miyamoto, K., 2018. Acceleration of enzymatic degradation of poly(ethylene terephthalate) by surface coating with anionic surfactants. ChemSusChem 11, 4018–4025. https://doi.org/10.1002/cssc.201802096.

Geyer, R., Jambeck, J.R., Law, K.L., 2017. Production, use, and fate of all plastics ever made. Sci. Adv. 3. https://doi.org/10.1126/sciadv.1700782.

Harasymchuk, I., Kočí, V., Vitvarová, M., 2024. Chemical recycling: comprehensive overview of methods and technologies. Int. J. Sustain. Eng. 17, 124–148. https://doi.org/10.1080/19397038.2024.2409162.

Hocker, S., Rhudy, A.K., Ginsburg, G., Kranbuehl, D.E., 2014. Polyamide hydrolysis accelerated by small weak organic acids. Polymer (Guildf). 55, 5057–5064. https://doi.org/10.1016/j.polymer.2014.08.010.

Iroegbu, A.O.C., Ray, S.S., Mbarane, V., Bordado, J.C., Sardinha, J.P., 2021. Plastic pollution: a perspective on matters arising: challenges and opportunities. ACS Omega. https://doi.org/10.1021/acsomega.1c02760.

Iwaya, T., Sasaki, M., Goto, M., 2006. Kinetic analysis for hydrothermal depolymerization of nylon 6. Polym. Degrad. Stab. 91, 1989–1995. https://doi.org/10.1016/j.polymdegradstab.2006.02.009.

Jaime-Azuara, A., Longo, E., Boselli, E., Baratieri, M., Pedersen, T.H., 2024. Exploratory DSC investigation on the solvolytic depolymerization of PET in varied solvent systems and in the presence of model additives and contaminants. Polym. Degrad. Stab. 224. https://doi.org/10.1016/j.polymdegradstab.2024.110751.

Jaime-Azuara, A., Pedersen, T.H., Wimmer, R., 2023. Process optimization by NMR-assisted investigation of chemical pathways during depolymerization of PET in subcritical water. Green Chem. 25, 2711–2722. https://doi.org/10.1039/d2gc04831k.

Laredo, G.C., Reza, J., Meneses Ruiz, E., 2023. Hydrothermal liquefaction processes for plastics recycling: a review. Clean. Chem. Eng. 5, 100094. https://doi.org/10.1016/j.clce.2023.100094.

Lee, H.L., Chiu, C.W., Lee, T., 2021. Engineering terephthalic acid product from recycling of PET bottles waste for downstream operations. Chem. Eng. J. Adv. 5. https://doi.org/10.1016/j.ceja.2020.100079.

Matayeva, A., Biller, P., 2022. Hydrothermal liquefaction of post-consumer mixed textile waste for recovery of bio-oil and terephthalic acid. Resour. Conserv. Recycl. 185, 106502. https://doi.org/10.1016/J.RESCONREC.2022.106502.

Matayeva, A., Biller, P., 2021. Hydrothermal liquefaction aqueous phase treatment and hydrogen production using electro-oxidation. Energy Convers. Manag. 244. https://doi.org/10.1016/j.enconman.2021.114462.

Matayeva, A., dos Passos, J.S., Straka, P., Skibsted, S.K.G., Biller, P., 2025. Chemical recycling of post-consumer textile waste via continuous hydrothermal liquefaction and hydrotreatment for simultaneous monomer and hydrocarbons production. Chem. Eng. J. 508. https://doi.org/10.1016/j.cej.2025.161108.

Matayeva, A., Madsen, A.S., Biller, P., 2023. Evaluation of different fiber impurities on hydrothermal liquefaction of mixed textile waste. Resour. Conserv. Recycl. 190. https://doi.org/10.1016/j.resconrec.2022.106833.

Minor, A.J., Goldhahn, R., Rihko-Struckmann, L., Sundmacher, K., 2023. Chemical recycling processes of nylon 6 to caprolactam: review and techno-economic assessment. Chem. Eng. J. 474. https://doi.org/10.1016/j.cej.2023.145333.

Nouira, A., Bekri-Abbes, I., Cansado, I.P.P., Mourão, P.A.M., 2025. Taguchi robust design of phase transfer catalytic hydrolysis of polyethylene terephthalate (PET) waste in mild conditions: application for the preparation of metal–organic frameworks. Solids 6. https://doi.org/10.3390/solids6010010.

Parnell, K., Rolston, A., Hilton, B., Luccitti, A., 2025. Circular economy in the textile industry: a review of technology, practice, and opportunity. Recycling. https://doi.org/10.3390/recycling10060225.

Patkar, M., Jabarin, S.A., 1993. Effect of Diethylene Glycol (DEG) on the Crystallization Behavior of Poly (ethylene terephthalate) (PET), Journal of Applied Polymer Science. John Wiley & Sons, Inc.

Peti, D., Dobránsky, J., Michalík, P., 2025. Recent advances in polymer recycling: a review of chemical and biological processes for sustainable solutions. Polymers (Basel). https://doi.org/10.3390/polym17050603.

PLASTIC EUROPE, 2025. Plastics the Fast Facts 2025 [WWW Document]. URL https://plasticseurope.org/ (Accessed 2.27.26).

PLASTIC EUROPE, 2022. Plastics - the Facts 2022 [WWW Document]. URL https://plasticseurope.org/ (Accessed 2.27.26).

Ragaert, K., Delva, L., Van Geem, K., 2017. Mechanical and chemical recycling of solid plastic waste. Waste Manage. 69, 24–58. https://doi.org/10.1016/j.wasman.2017.07.044.

Sato, O., Arai, K., Shirai, M., 2006. Hydrolysis of poly(ethylene terephthalate) and poly (ethylene 2,6-naphthalene dicarboxylate) using water at high temperature: effect of proton on low ethylene glycol yield. Catal. Today. 297–301. https://doi.org/10.1016/j.cattod.2005.10.040.

Savage, P.E., 2024. Renewable fuels and chemical recycling of plastics via hydrothermal liquefaction. Acc. Chem. Res. 57, 3386–3396. https://doi.org/10.1021/acs.accounts.4c00524.

Schirmeister, C.G., Mülhaupt, R., 2022. Closing the carbon loop in the circular plastics economy. Macromol. Rapid Commun. https://doi.org/10.1002/marc.202200247.

Seshasayee, M.S., Savage, P.E., 2020. Oil from plastic via hydrothermal liquefaction: production and characterization. Appl. Energy 278. https://doi.org/10.1016/j.apenergy.2020.115673.

Snowden-Swan, L.J., Hallen, R.T., Zhu, Y., Billing, J.M., Jones, S.B., Hart, T.R., Elliott, D. C., Fox, S.P., Schmidt, A.J., Maupin, G.D., 2016. Hydrothermal Liquefaction and Upgrading of Municipal Wastewater Treatment Plant Sludge: A Preliminary Techno-Economic Analysis.

Stiegelmaier, E., Costa, T.C., Pakuszewski, G., Ulson, G., de Souza, S.M.A., Ulson de Souza, A.A., Serafini Immich, A.P., 2024. Enhancing polyamide 6: Acid hydrolysis for functionalization and amino group quantification. Polymer (Guildf). 298. https://doi.org/10.1016/j.polymer.2024.126905.

Textile Exchange, 2024. Textile Exchange - Materials Market Report.

Tito, E., dos Passos, J.S., Bensaid, S., Pirone, R., Biller, P., 2023. Multilayer plastic film chemical recycling via sequential hydrothermal liquefaction. Resour. Conserv. Recycl. 197. https://doi.org/10.1016/j.resconrec.2023.107067.

Tito, E., dos Passos, J.S., Rombolà, A.G., Torri, C., Bensaid, S., Pirone, R., Biller, P., 2024. Sequential hydrothermal dechlorination and liquefaction of PVC. Energy Convers. Manag. 304. https://doi.org/10.1016/j.enconman.2024.118228.

Umdagas, L., Orozco, R., Kings, I., Thom, W., Al-Duri, B., 2026. Advances in chemical recycling of polyolefins by hydrothermal liquefaction in supercritical water: a comprehensive review. J. Supercrit. Fluids. https://doi.org/10.1016/j.supflu.2025.106761.

Van Geem, K.M., 2023. Plastic waste recycling is gaining momentum. Science (1979). 381, 607–608. 10.1126/science.adj2807.

Yu, J., Wang, X., Hu, H., Xu, Q., Sun, L., Zhu, R., Gao, T., He, Y., Ma, B., 2023. 1Rapid hydrolysis of waste and scrap PA6 textiles to ε–caprolactam. ACS Appl. Polym. Mater. 5, 751–763. https://doi.org/10.1021/ACSAPM.2C01744.

Yu, Y., Zhang, Y., Zhu, S., Mei, Q., 2025. Cost-effective and low-carbon scalable recycling of waste polyethylene terephthalate through bio-based guaiacol-enhanced methanolysis. Angew. Chem. Int. Ed. 64. https://doi.org/10.1002/anie.202503469.